Supplementary Material for "A shady phytoplankton paradox: When phytoplankton increases under low light."

Masato Yamamichi, Takehiro Kazama, Kotaro Tokita, Izumi Katano, Hideyuki Doi, Takehito Yoshida, Nelson G. Hairston Jr., & Jotaro Urabe

Proceedings of the Royal Society B: Biological Sciences

Appendix S1: Chemical analyses and enumeration of plankton

We collected duplicate 10-L pond water sample from the bottom to surface by repeated deployment of a 2.2-L tube sampler from floating docks deployed in each pond (Fig. 1). The water samples were kept in the dark and brought to the laboratory within two hours, and used for quantifying dissolved and particulate organic (seston) matter, chlorophyll *a* concentration, and phytoplankton biomass and composition. We measured dissolved oxygen (DO) concentration using a multi-probe sonde (556MPS; YSI, Yellow Springs, U.S.A.) from the floating docks.

To collect zooplankton, we took samples at 5 sites along a diagonal line in each pond. A 22 L water sample from each pond was filtered using a 100 μm mesh net, and fixed with 99% ethanol. Zooplankton samples were concentrated into 20 mL plastic vials and stored at 4°C.

Submersed macrophytes were collected in triplicate on August 16, 2015 using an Ekman-Birge grab sampler (15×15 cm) around the floating docks. To quantify the area dominated by submersed macrophytes, we took photos of the six experimental ponds from above using an unmanned aerial vehicle (UAV) with a video camera (Phantom 3, DJI, Shenzhen, China) on October 7, 2015 after the experiment had been terminated and the floating swimming-pool covers removed. All images were analyzed using ImageJ software

(Schneider et al. 2012). For each image, the area dominated by submersed macrophytes was distinguished as dark-green color whereas bare pond bottoms were distinguished as bright-brown color after contrast enhancement. The area dominated by submersed macrophytes and pond surface were outlined manually, and measured area using the "Measure" function in ImageJ. Submersed macrophyte coverage was evaluated as a fraction of total pond surface area.

For quantifying seston C, N, and P, 50 mL samples were filtered onto pre-combusted GF/F glass fiber filters (GE Healthcare, U.K. Inc., Little Chalfont, England), and dried in a desiccator. Seston C and N were determined with a CN analyzer (model 2400; Perkin-Elmer, Inc., Waltham, U.S.A.). Seston P was determined by the ascorbate-reduced molybdenum-blue method after digestion with potassium persulfate at 120°C for 30 minutes (American Public Health Association 1989). For determination of total dissolved N (TDN) and soluble reactive phosphorus (SRP), water samples were filtrated by GF/F, and immediately frozen and stored at –20°C. TDN was analyzed with a TOC/TN analyzer (multi N/C 3100; Analytik Jena AG, Jena, Germany). SRP was determined by the ascorbic acid modification of the molybdenum blue method (American Public Health Association 1989). For determination of chlorophyll *a* concentration, a 50 mL of aliquot of a sample was filtered

onto a GF/F glass filter. Filters were immediately frozen and stored at –20°C. Chlorophyll *a* was extracted in 90% ethanol for 24 hours in the dark and measured using a fluorometer (10-AU; Turner Designs, Inc., San Jose, U.S.A.), as described in Sartory and Grobbelaar (1984).

Because of the short generation times of phytoplankton, we used total (seston plus dissolved) nitrogen (TN) and total phosphorus (TP) as a surrogate for the amount of nutrient loading to aquatic ecosystems as described in Sterner et al. (1997). TN and TP were calculated by TDN plus seston N and SRP plus seston P, respectively. Mean concentration of total- and sestonic matter and chlorophyll *a* for each pond were calculated from duplicate samples of the biweekly sampling.

For phytoplankton, we preserved 50 mL subsamples with Lugol's solution (final concentration, 5% in 2015 and 1% in 2016). After settling for 24 hours, we removed supernatant by siphoning and concentrated to 10–20 mL. One to five milliliters of subsample was analyzed from each concentrated sample. All phytoplankton cells were enumerated at the finest taxon level (species or genus), and cell dimension was measured on 10 to 30 cells of each algal taxon under a microscope at 200 to 400× magnification. Taxa were classified into eight groups (Cryptophyceae, Crysophyceae, Cyanobacteria, Dinophyceae, Bacillariophyceae

(diatoms), Chlorophyceae (green algae), Euglenophyceae, and "other"). Mean cell volumes were estimated from the cell dimensions applied to common geometric shapes according to functions by Willén (1976), Sun and Liu (2003), and Olenina et al. (2006). Then, phytoplankton biovolume was estimated from the mean cell volume and density of each algal taxa.

For zooplankton identification and enumeration, 1 – 4 mL subsamples were analyzed from each concentrated sample. Cladocerans and copepods were identified according to Thorp and Covich (1991) and enumerated at least total 200 individuals in qualitative analysis with measurements of the body lengths under a microscope at 25 to 72× magnification. Zooplankton body mass for each taxon was estimated using length-weight regression equations from McCauley (1984).

We monitored the photon flux density (μmol m^{-2} s^{-1}) above and below the water surface at each pond by using spherical quantum sensor (LI-193; LiCor, Inc.) between 10 am and 12 am at the biweekly sampling. We determined the light attenuation coefficients, λ (m^{-1}), by fitting an exponential function, $I_z = I_0\exp(-\lambda z)$, where z is depth (m), I_z and I_0 are observed photon flux densities at z and 0 m depth. According to McCree (1972), we assumed that 4.57 μmol m^{-2} s^{-1} in photon flux density is 1 J m^{-2} s^{-1} in irradiance (Table S2).

When we surveyed the 35 CUEPF ponds in 2016, we collected 7-L of sub-surface pond water (<50 cm from surface) by repeated towing of a 1.4-L weighted PET bottle from the shore at each pond. For chlorophyll *a*, we filtrated 50 mL of aliquot onto a GF/F glass filter, and stored immediately at –4°C in dark. Chlorophyll *a* concentration was quantified by the same method described above. For macrophytes, we took aerial photos by an UAV and measured the fraction of macrophytes coverage area (0 to 100% of pond area) as a proxy of macrophytes abundance with ImageJ (Schneider et al. 2012) because those were significantly correlated in our six experimental ponds in 2015 (Fig. S2).

References

American Public Health Association. 1989. Standard Methods for the Examination of Water and Wastewater. American Public Health Association, Washington, D.C., U.S.A.

Hwang, S. J., K. E. Havens, and A. D. Steinman. 1998. Phosphorus kinetics of planktonic and benthic assemblages in a shallow subtropical lake. Freshwater Biology **40**:729-745.

Jäger, C. G., and S. Diehl. 2014. Resource competition across habitat boundaries: asymmetric interactions between benthic and pelagic producers. Ecological Monographs **84**:287-302.

McCauley, E. 1984. The estimation of the abundance and biomass of zooplankton in samples. Pages 228-265 *in* J. A. Downing and F. H. Rigler, editors. A manual on methods for the assessment of secondary productivity in fresh waters. Blackwell Scientific Publications, Oxford, U.K.

McCree, K. J. 1972. Test of current definitions of photosynthetically active radiation against leaf photosynthesis data. Agricultural Meteorology **10**:443-453.

Muhammetoğlu, A. B., and S. Soyupak. 2000. A three-dimensional water quality-macrophyte interaction model for shallow lakes. Ecological Modelling **133**:161-180.

Mulderij, G., E. H. Van Nes, and E. Van Donk. 2007. Macrophyte–phytoplankton interactions: the relative importance of allelopathy versus other factors. Ecological Modelling **204**:85-92.

Olenina, I., S. Hajdu, L. Edler, A. Andersson, N. Wasmund, S. Busch, J. Göbel, S. Gromisz, S. Huseby, M. Huttunen, A. Jaanus, P. Kokkonen, I. Ledaine, and E. Niemkiewicz. 2006. Biovolumes and size-classes of phytoplankton in the Baltic Sea. HELCOM Baltic Sea Environment Proceedings **106**:1-144.

Sartory, D. P., and J. U. Grobbelaar. 1984. Extraction of chlorophyll *a* from freshwater phytoplankton for spectrophotometric analysis. Hydrobiologia **114**:177-187.

Schneider, C. A., W. S. Rasband, and K. W. Eliceiri. 2012. NIH Image to ImageJ: 25 years of image analysis. Nature Methods **9**:671-675.

Sterner, R. W., J. J. Elser, E. J. Fee, S. J. Guildford, and T. H. Chrzanowski. 1997. The light:nutrient ratio in lakes: The balance of energy and materials affects ecosystem structure and process. American Naturalist **150**:663-684.

Sun, J., and D. Liu. 2003. Geometric models for calculating cell biovolume and surface area for phytoplankton. Journal of plankton research **25**:1331-1346.

Thorp, J. H., and A. P. Covich. 1991. Ecology and Classification of North American Freshwater Invertebrates. Academic Press, San Diego, CA.

van Gerven, L. P. A., J. J. M. de Klein, D. J. Gerla, B. W. Kooi, J. J. Kuiper, and W. M. Mooij. 2015. Competition for light and nutrients in layered communities of aquatic plants. The American Naturalist **186**:72-83.

Willén, E. 1976. A simplified method of phytoplankton counting. British Phycological Journal **11**:265-278.

Table S1. The number of individuals and total wet weight (g WW) of introduced largemouth bass.

Pond ID	Number of fish	Total weight (g WW)
203 (control)	5	91
217 (control)	6	115
204 (medium)	6	91
218 (medium)	6	77
202 (low)	6	103
219 (low)	6	97

Table S2. Parameter descriptions and default values. *A*: pelagic algae (phytoplankton), *S*: submersed macrophytes. Reference 1: Mulderij et al. (2007), 2: van Gerven et al. (2015), 3: Hwang et al. (1998) , 4: Muhammetoğlu and Soyupak (2000) , 5: Jäger and Diehl (2014), FO: field observation, ARV: arbitrary realistic value. *Light was converted by assuming 4.57 μmol m^{-2} s^{-1} = 1 J m^{-2} s^{-1}. ¶We assumed that 2 g P (N)/g C = 1 g P (N)/g DW.

Parameter	Description	Unit	Value	Reference
$p_{max,A}$	Maximum growth rate of *A*	day^{-1}	.5	(1)
$p_{max,S}$	Maximum growth rate of *S*	day^{-1}	.3	(2)
M_A	Half-saturation constant for nutrient of *A*	g P (N) m^{-3}	.003 (.025)	(1), (5)
M_S	Half-saturation constant for nutrient of *S*	g P (N) m^{-3}	.003 (.01)	(3), (4)
m_A	Loss rate of *A*	day^{-1}	.1	(1), (5)
m_S	Loss rate of *S*	day^{-1}	.1	ARV
k_A	Light attenuation coefficient of *A*	m^2 g DW^{-1}	.2	(1)
k_S	Light attenuation coefficient of *S*	m^2 g DW^{-1}	.02	(1)
H_A	Half-saturation constant for light of *A*	μmol m^{-2} s^{-1}	30	(1)
H_S	Half-saturation constant for light of *S*	μmol m^{-2} s^{-1}	150	(2)*
c_A	Nutrient to dry weight ratio of *A*	g P (N) g DW^{-1}	.01 (.13)	(1)¶
c_S	Nutrient to dry weight ratio of *S*	g P (N) g DW^{-1}	.005 (.02)	ARV, (2)
R_{in}	Nutrient concentration in sediment	g P (N) m^{-3}	.3 (3)	(1)
I_{in}	Incoming light intensity	μmol m^{-2} s^{-1}	0-1000	Variable
z_1	Depth of the pelagic habitat	m	1.4	FO

z_2	Depth of the benthic habitat	m	.1	FO
q	Nutrient loading rate	m day^{-1}	.05	(5)
a	Exchange rate of A and nutrient	m day^{-1}	.05	(5)
K_{bg}	Background light attenuation	m^{-1}	.2	(1)

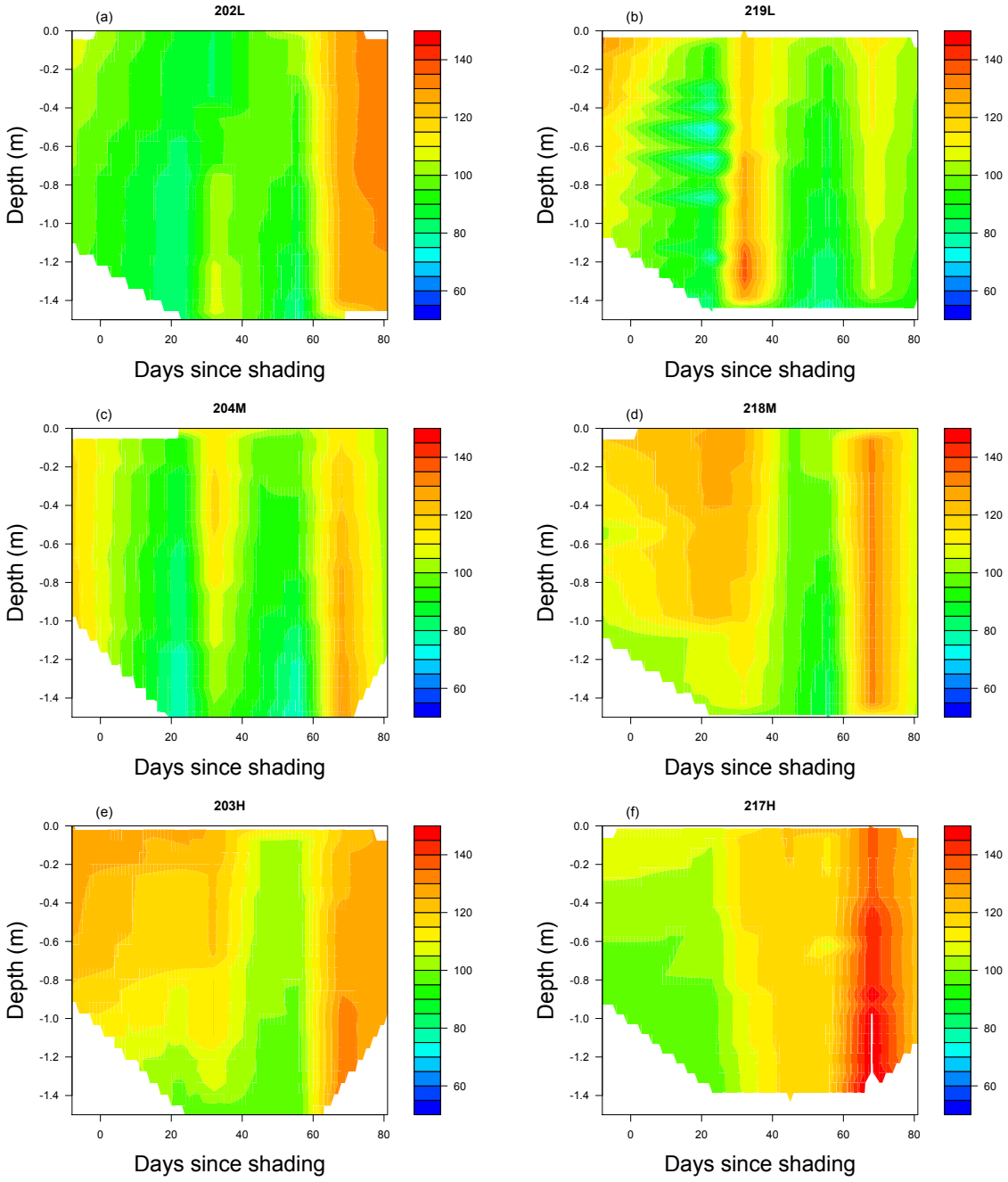

Figure S1. Contour plots of dissolved oxygen (DO) saturation level (%) in the ponds. X axes are days since shading (July 3, 2015) and Y axes are depth (m) from surface (0 m) to bottom (ca. 1.5 m). Contours were calculated by the "interp" function of the "akima" package in R.

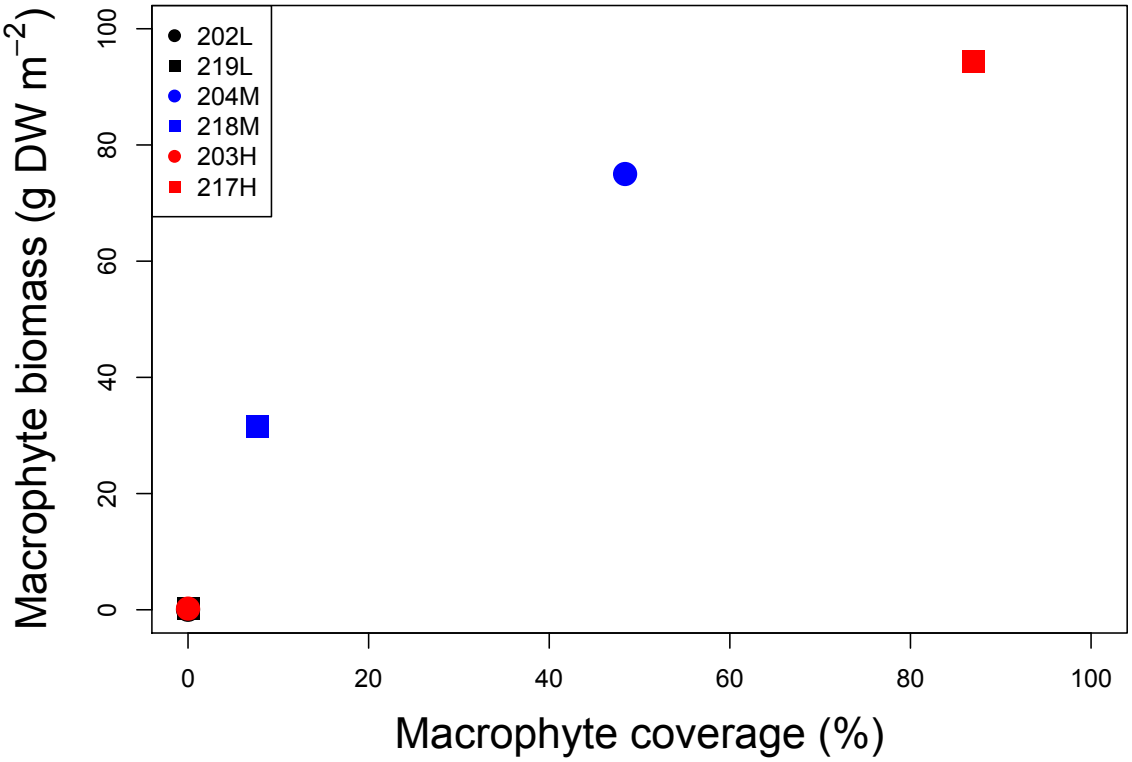

Figure S2. A relationship between submersed macrophyte coverage (%) and submersed macrophyte biomass (g DW m^{-2}). Ponds 202 (low-light), 203 (control), and 219 (low-light) are overlapping at the origin on this figure. A Spearman's rank correlation coefficient, ρ = 0.95 (P = 0.0030).

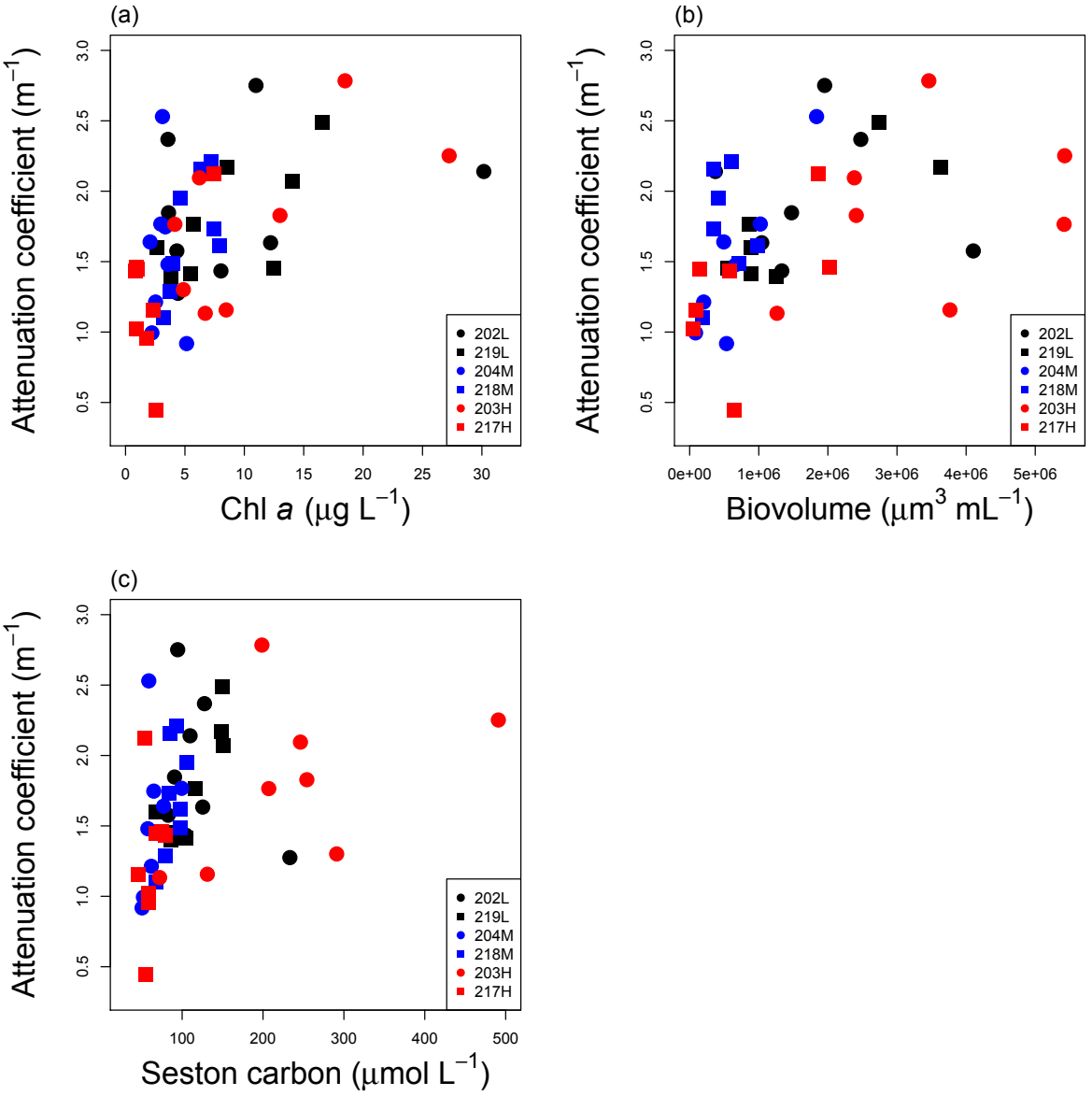

Figure S3. Relationships between attenuation coefficients (m^{-1}) and chlorophyll *a* ($\mu g\ L^{-1}$) (a), total biovolume of phytoplankton ($\mu m^3\ mL^{-1}$) (b), and seston carbon ($\mu mol\ L^{-1}$) (c). Data were from June 24 to September 21, 2015 (please note that we did not measure biovolume on August 16). Spearman's rank correlation coefficients (ρ) were 0.51 ($P = 0.00021$), 0.50 ($P = 0.00098$), and 0.51 ($P = 0.00030$) for chlorophyll *a*, biovolume, and seston carbon, respectively.

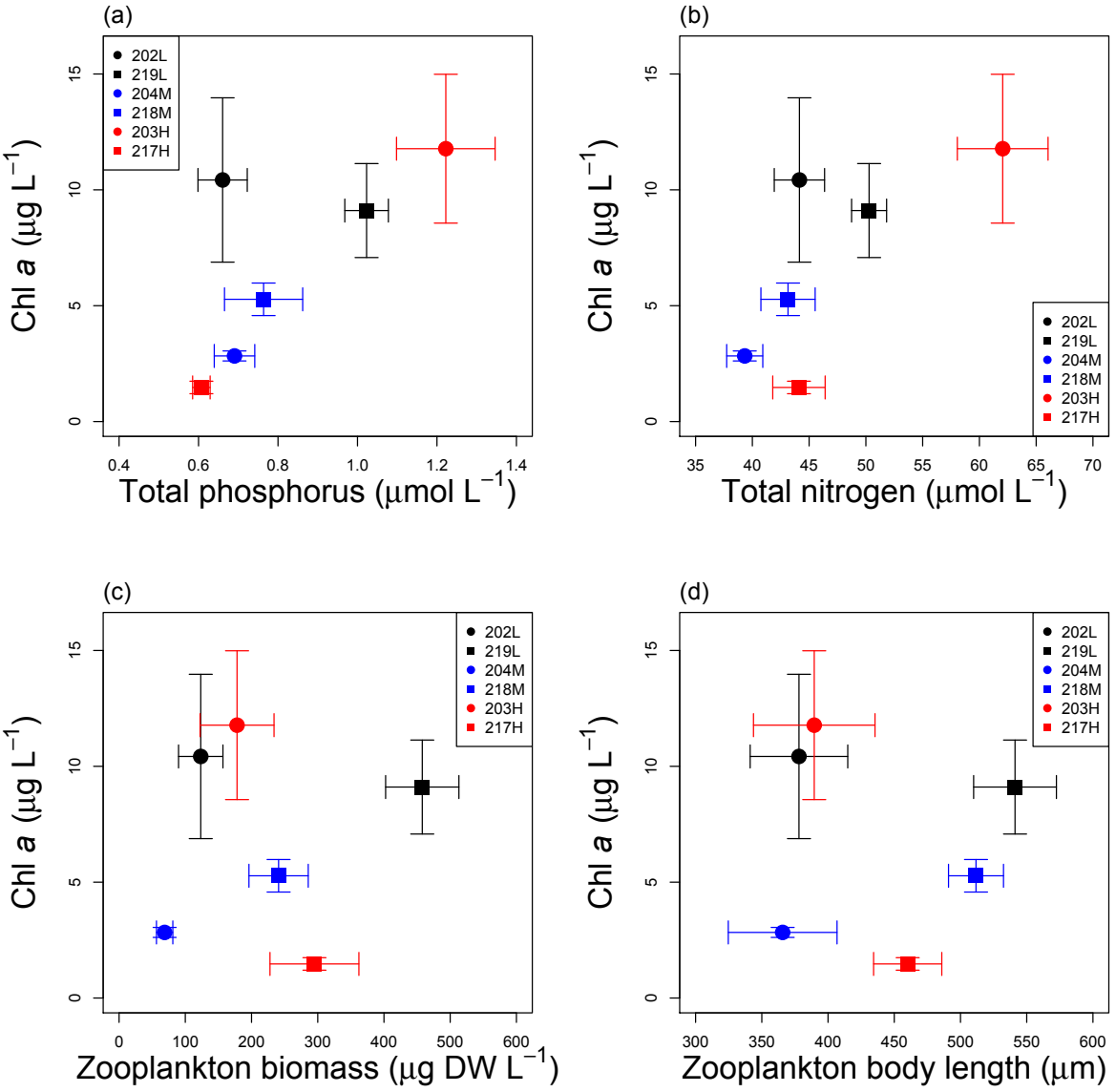

Figure S4. Relationships between chlorophyll *a* (µg L^{-1}) and total phosphorus (µmol L^{-1}, TP) (a), total nitrogen (µmol L^{-1}, TN) (b), zooplankton biomass (µg DW L^{-1}) (c), and zooplankton body length (µm) (d) from July 10 to September 21, 2015 (mean and standard error). Spearman's rank correlation coefficients (ρ) between the mean values of each pond were 0.66 ($P = 0.18$), 0.77 ($P = 0.10$), –0.14 ($P = 0.80$), and –0.029 ($P > 0.99$) for TP, TN, zooplankton biomass, and zooplankton body length, respectively.

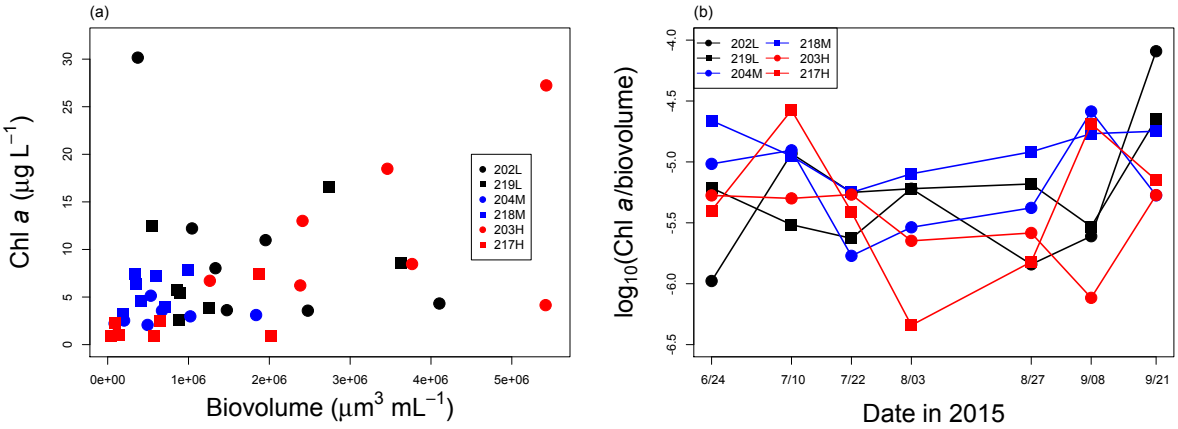

Figure S5. (a) A relationship between total biovolume of phytoplankton (µm^3 mL^{-1}) and chlorophyll *a* (µg L^{-1}). A Spearman's rank correlation coefficient between measurements from each sampling date, ρ = 0.46 (P = 0.0020). (b) Time-series of chlorophyll *a*/total biovolume of phytoplankton from June 24 to September 21, 2015. Please note that we did not measure biovolume on August 16.

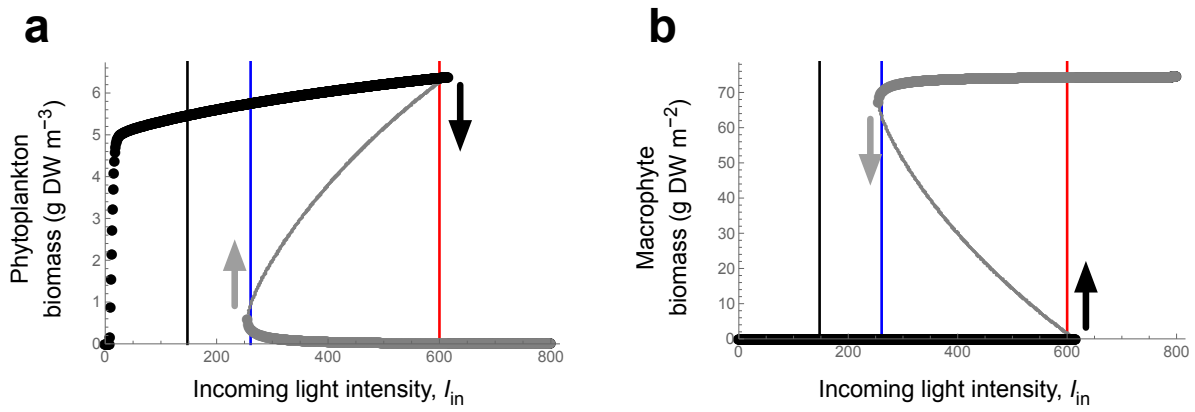

Figure S6. Bifurcation analyses based on the parameters for nitrogen (Table S2). Y axes of (a) and (b) show phytoplankton biomass (the phytoplankton concentration in the entire water column averaged over the pelagic and benthic habitats, $(z_1A_1 + z_2A_2)/(z_1 + z_2)$, g DW m^{-3}) and submersed macrophyte biomass (z_2S, g DW m^{-2}), respectively, along incoming light intensity (I_{in}). Abrupt shifts were indicated by black and gray arrows. Black and gray dots represent stable equilibria, and gray small dots represent unstable equilibria. Red, blue, and black vertical lines indicate light conditions for control, medium-light, and low-light ponds, respectively when the light intensity of control ponds is assumed to be 600 (μmol m^{-2} s^{-1}).

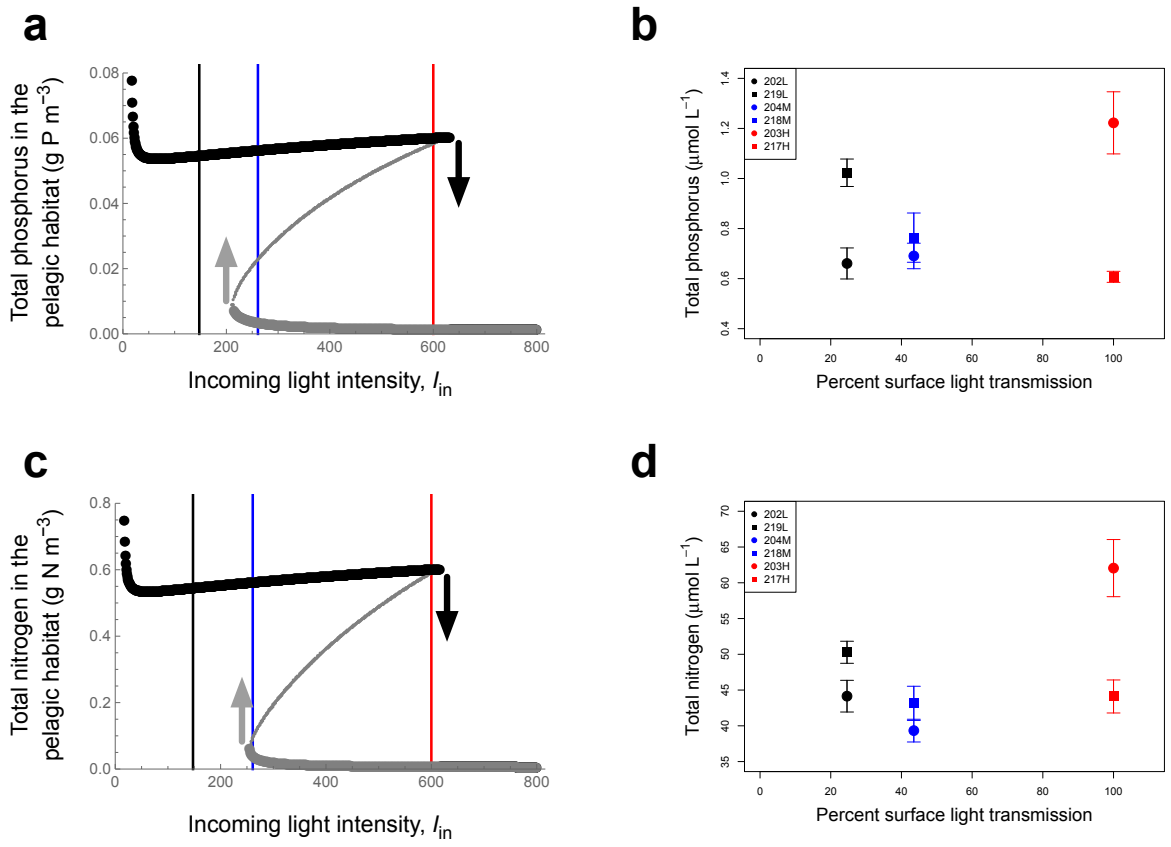

Figure S7. Bifurcation plots of nutrients in the pelagic habitat. Bifurcation analyses of the model demonstrate that decreasing surface light gradually increases nutrients (phosphorus and nitrogen) in the pelagic habitat ($R_1 + c_A A_1$) followed by an abrupt shift (indicated by gray arrows) due to alternative stable states (Figs. S7a, S7b). Increasing light can also cause the abrupt shift in nutrients (black arrows). This is consistent with our experimental results (Figs. S7b, S7d) and the observed positive correlation between biomass of phytoplankton and nutrients (Figs. S4a, S4b). Black and gray dots represent stable equilibria and smaller gray dots represent unstable equilibria. Red, blue, and black vertical lines indicate light conditions for control, medium-light, and low-light ponds, respectively when the light intensity of control ponds is assumed to be 600 (µmol m^{-2} s^{-1}).

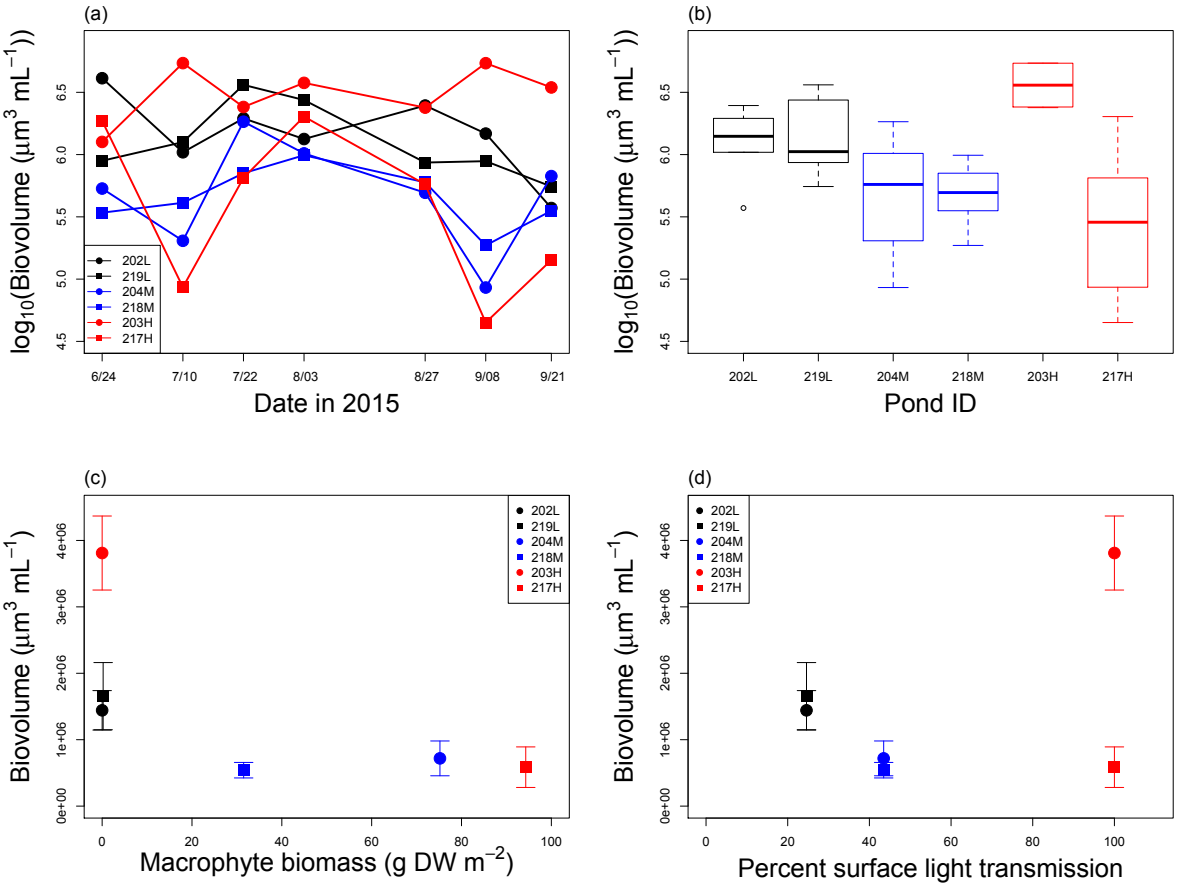

Figure S8. (a) Time-series of total biovolume of phytoplankton (μm^3 mL^{-1}) from June 24 to September 21, 2015. Please note that we did not measure biovolume on August 16. (b) Boxplot of total biovolume of phytoplankton under three light intensities from July 10 to September 21, 2015. The bold line in the box indicates the median value. Lower/upper limits of the box are the first/third quartiles, respectively. Lower/upper whisker plots represent the minimum/maximum values within the first/third quartiles minus/plus 1.5 × interquartile range, respectively. (c) A correlation between total biovolume of phytoplankton (mean and standard error, SE) and submersed macrophyte biomass on August 16, 2015 (A Spearman's rank

correlation coefficient (ρ) was –0.73 with $P = 0.10$). Red: control, blue: medium-light, black: low-light. Circle: road-side ponds, square: channel-side ponds. Error bars indicate SE values. (d) A relationship between surface uncovered (%) and total biovolume of phytoplankton.

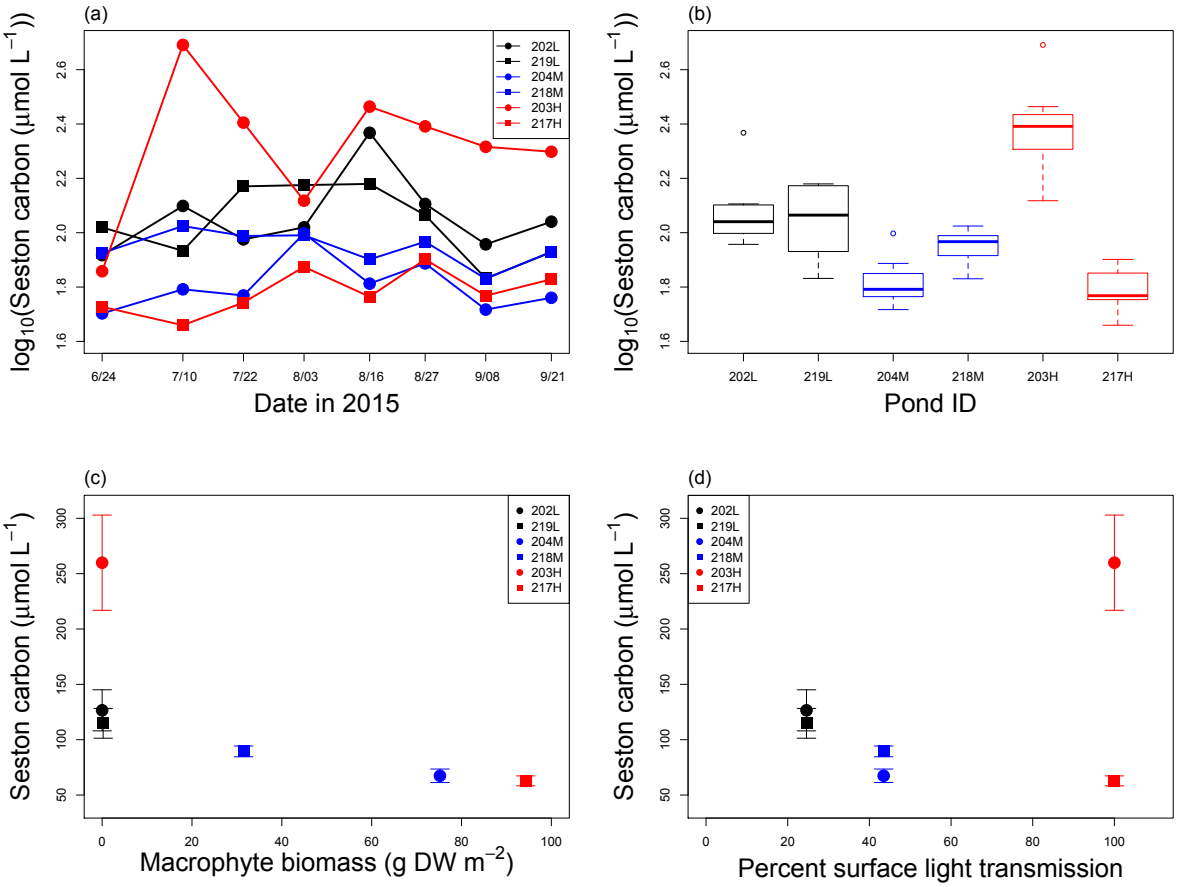

Figure S9. (a) Time-series of seston carbon (µmol L^{-1}) from June 24 to September 21, 2015. (b) Boxplot of seston carbon under three light intensities from July 10 to September 21, 2015. The bold line in the box indicates the median value. Lower/upper limits of the box are the first/third quartiles, respectively. Lower/upper whisker plots represent the minimum/maximum values within the first/third quartiles minus/plus 1.5 × interquartile range, respectively. (c) A correlation between seston carbon (mean and SE) and submersed macrophyte biomass on August 16, 2015 (A Spearman's rank correlation coefficient (ρ) was –0.99 with P = 0.00031). Red: control, blue: medium-light, black: low-light. Circle: road-side

ponds, square: channel-side ponds. Error bars indicate SE values. (d) A relationship between surface uncovered (%) and seston carbon.

Figure S10. Phytoplankton biomass (μm^3 mL^{-1}) composition changes during the experiment in 2015. Green: green algae (Chlorophyceae), pale green: diatoms (Bacillariophyceae), blue: cyanobacteria, purple: Euglenophyceae, orange: Cryptophyceae, red: Dinophyceae, yellow: Chrysophyceae, pink: others.

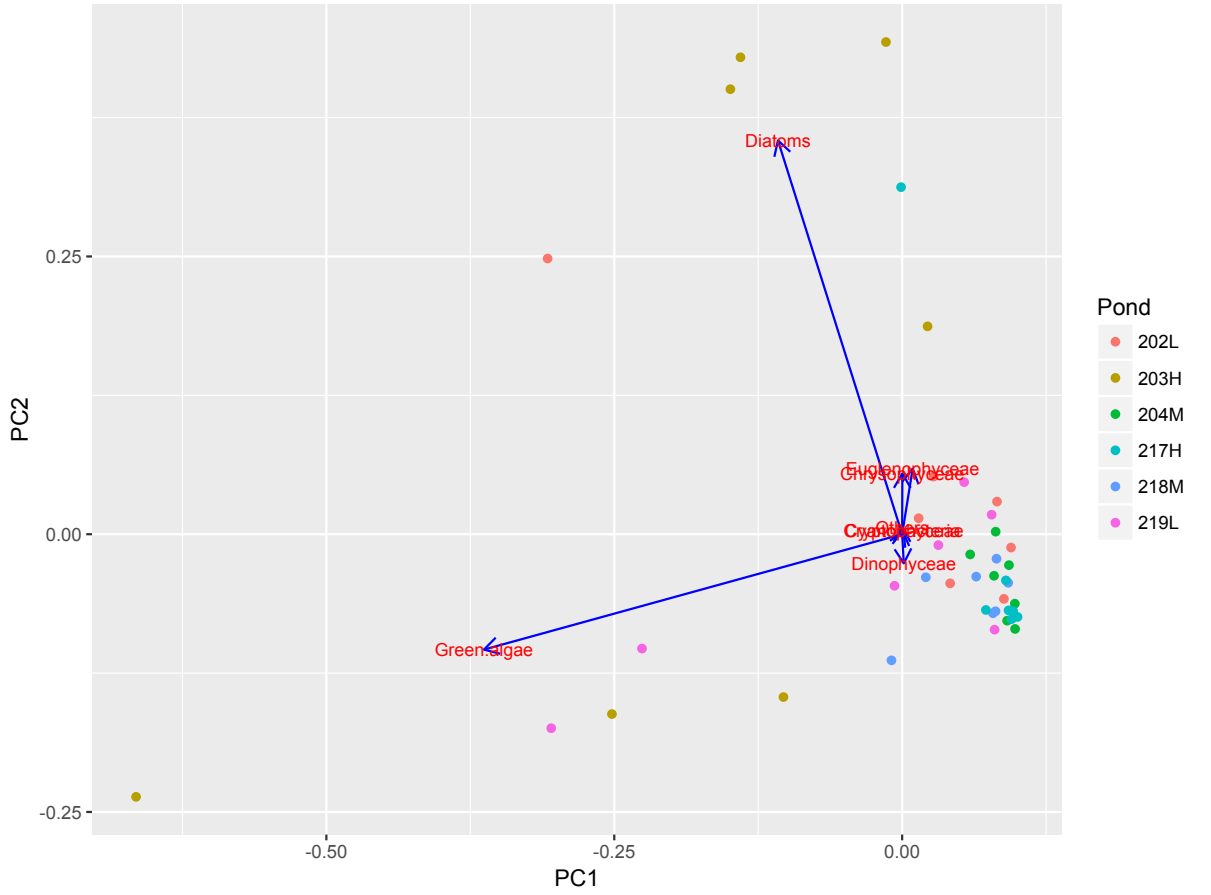

Figure S11. Principle component analysis (PCA) of phytoplankton biomass dynamics (Fig. S10). Eigenvectors are shown by blue arrows. PCA was performed using the "prcomp" function and visualized by the "autoplot" function of the "ggfortify" package in R.

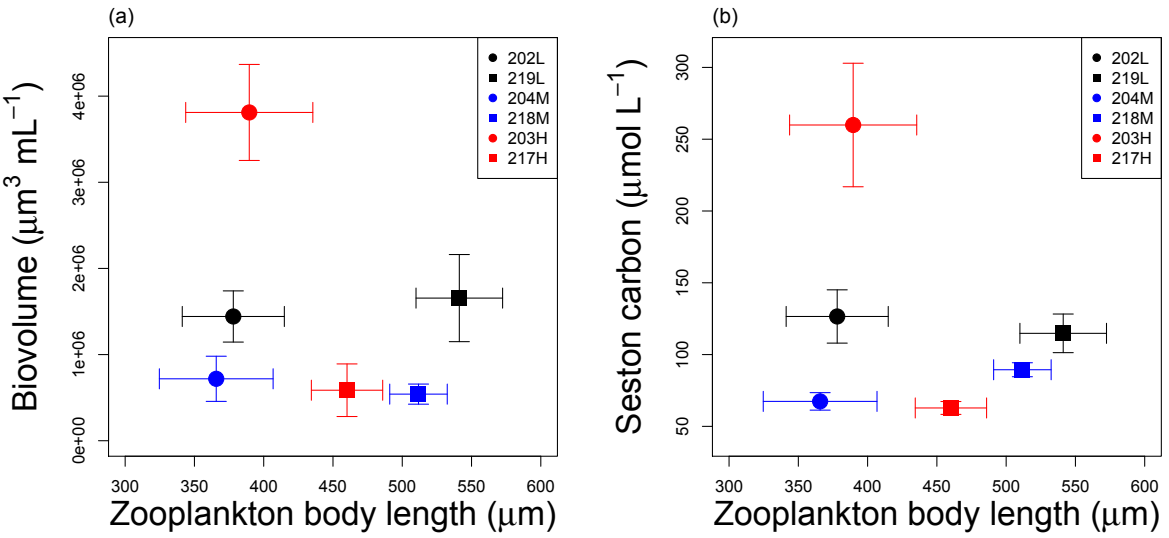

Figure S12. Relationships between zooplankton body length (µm) and total biovolume of phytoplankton (µm^3 mL^{-1}) (a) and seston carbon (µmol L^{-1}) (b) from July 10 to September 21, 2015 (mean and standard error). Spearman's rank correlation coefficients (ρ) between the mean values of each pond were –0.086 (P = 0.92), and –0.029 (P > 0.99) for total biovolume of phytoplankton and seston carbon, respectively.